Optimized Metal–Organic-Framework Nanospheres for Drug Delivery: Evaluation of Small-Molecule Encapsulation

Jia Zhuang,[†] Chun-Hong Kuo,[†] Lien-Yang Chou,[†] De-Yu Liu,[‡] Eranthie Weerapana,[†,*] and Chia-Kuang Tsung[†,*]

[†]Department of Chemistry, Merkert Chemistry Center, Boston College, Chestnut Hill, Massachusetts 02467, United States, and [‡]Department of Chemistry and Biochemistry, University of California, Santa Barbara, California 93106, United States

ABSTRACT We have developed a general synthetic route to encapsulate small molecules in monodisperse zeolitic imid-azolate framework-8 (ZIF-8) nanospheres for drug delivery. Electron microscopy, powder X-ray diffraction, and elemental analysis show that the small-molecule-encapsulated ZIF-8 nanospheres are uniform 70 nm particles with single-crystalline structure. Several small molecules, including fluorescein and the anticancer drug camptothecin, were encapsulated inside of the ZIF-8 framework. Evaluation of fluorescein-encapsulated ZIF-8 nanospheres in the MCF-7 breast cancer cell line demonstrated cell internalization and minimal cytotoxicity. The 70 nm particle size facilitates cellular uptake, and the pH-responsive dissociation of the ZIF-8 framework likely results in endosomal release of the small-molecule cargo, thereby rendering the ZIF-8 scaffold an ideal drug delivery vehicle. To confirm this, we demonstrate that camptothecin encapsulated ZIF-8 particles show enhanced cell death, indicative of internalization and intracellular release of the drug. To demonstrate the versatility of this ZIF-8 system, iron oxide nanoparticles were also encapsulated into the ZIF-8 nanospheres, thereby endowing magnetic features to these nanospheres.

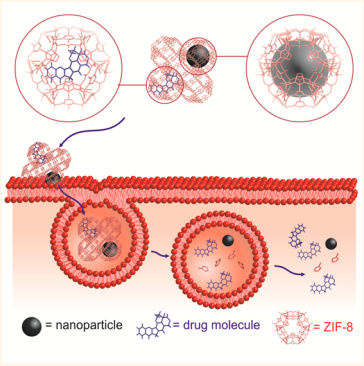

KEYWORDS: ZIF-8 · drug delivery · nanoparticles · cellular uptake

Direct administration of therapeutic agents to patients suffers from the intrinsic limitations of these small molecules including poor physiological stability, nonspecific targeting, and low cell-membrane permeability.[1] In many cases, high drug doses are necessary to offset the poor pharmacokinetics of these compounds, thereby increasing the potential of side effects. Nanomaterial drug carriers can overcome these limitations by stabilizing the drug through encapsulation or surface attachment,[2] facilitating cellular internalization, targeting delivery to a specific cell population,[3] and providing controlled release of the drug at the designated target.[4] Organic-based drug delivery systems (DDSs) including lipid- and polymer-based systems are approved for clinical use.[5] Recently, the use of inorganic nanomaterials in biological research represents one of the fastest growing areas[6] and inorganic-based DDSs have attracted attention due to tunable properties[7−11] that afford good biocompatibility,[12] ease of functionalization,[13] strong drug affinity,[14] and controllable release.[15]

Here, we developed a pH-responsive DDS with high cellular uptake efficiency by utilizing a nanosized metal organic framework (MOF), which possesses the advantages of both organic- and inorganic-based DDSs.[16] MOFs are crystalline porous compounds constructed of metal ions and organic linkers, and have been widely utilized in gas storage,[17,18] gas sensing,[19,20] chromatographic separation,[21,22] and heterogeneous catalysis.[23,24] Recently, MOFs have attracted attention for biomedical applications,[16] whereby metal ions have served as MRI contrast agents,[25,26] and organic linkers have been utilized as therapeutic molecules.[27] In our design, the three-dimensional MOF framework is used to encapsulate small molecules for intracellular delivery and subsequent release. Several pioneering studies demonstrate the great potential of MOF

* Address correspondence to eranthie@bc.edu, frank.tsung@bc.edu.

Received for review December 24, 2013 and accepted February 8, 2014.

Published online February 08, 2014
10.1021/nn406590q

DDSs,[28−35] yet further optimization is necessary to generate an optimal drug delivery carrier. (1) Size: previously reported MOFs are not monodisperse, or are larger than the optimal particle size (<100 nm) for cellular uptake.[33,36] (2) Stability: most MOFs are unstable under aqueous physiological conditions, leading to premature release or formation of large aggregates that decrease cellular uptake.[37] (3) Drug loading: many previous loading methods were based on equilibrium adsorption and diffusion, which results in inconsistencies.[28,38] (4) Biocompatibility: toxicity in biological systems needs to be minimized.[39] (5) Drug release: a limited number of release strategies have been successful in MOF-based materials.

To meet the prerequisites for an efficient DDS, we encapsulated small molecules into uniform and nanosized zeolitic imidazole framework-8 (ZIF-8) during synthesis. Our ZIF-8 nanospheres have uniform 70 nm size, which is optimal for cellular uptake and stable under aqueous physiological conditions. Drug loading is achieved under mild conditions and can be controlled by varying the amount of drug during particle synthesis. Due to the small window size of ZIF-8, the compounds are confined within the frameworks, thereby suppressing premature release. ZIF-8 is formed by 2-methyl imidazolate and zinc ions, which are components of physiological systems,[40] whereby zinc is the second most abundant transition metal in biology,[41] and the imidazole group is integral to the amino acid, histidine. The coordination between the zinc and imidazolate ions dissociates at pH 5.0−6.0;, which makes the drug release pH responsive and optimal for targeting cancer cells where extracellular microenvironments (pH 5.7−7.8) are more acidic than healthy tissues. Additionally, ZIF-8 nanospheres can be further functionalized through encapsulation of nanoparticles in the spheres,[24,42,43] modification of the linkers,[44,45] and surface grafting to target the drug to distinct cell populations.[26]

RESULTS AND DISCUSSION

We developed a synthetic method for nanosized ZIF-8 spheres and demonstrated encapsulation of small molecules into the frameworks during synthesis (Scheme 1). We first incorporated fluorescein, which is commonly used as a fluorescent "drug mimic" and is larger than the ZIF-8 window.

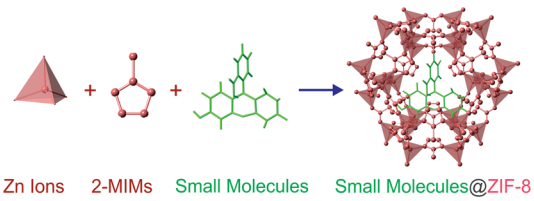

Scheme 1. Encapsulation of small molecules into the frameworks during synthesis.

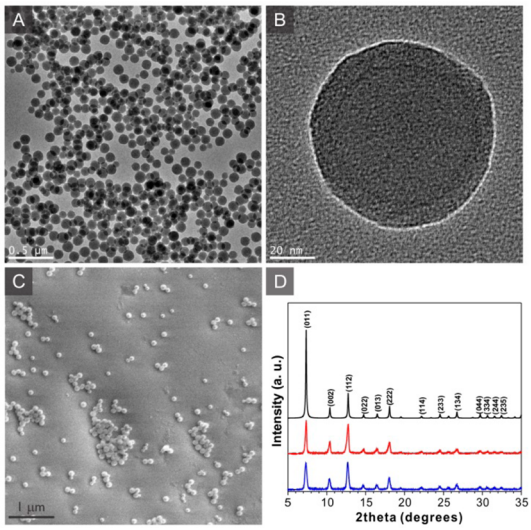

Figure 1. (A) TEM image of fluorescein-encapsulated ZIF-8 nanospheres; (B) zoom-in on a single nanosphere; (C) SEM image of fluorescein-encapsulated ZIF-8 nanospheres; (D) XRD patterns of pure ZIF-8 (blue), fluorescein-encapsulated ZIF-8 nanospheres (red), and simulated ZIF-8 patterns (black).

Small-molecule loading into the ZIF-8 frameworks, as well as cellular uptake, can be monitored by fluorescence. Fluorescein-encapsulated nanospheres were generated by mixing zinc nitrate and 2-methyl imidazole in the presence of fluorescein in methanol. The reaction mixture turned milky after 5 min, implying the formation of ZIF-8 nanospheres. SEM and TEM images of these ZIF-8 nanospheres (Figure 1A−C) identify monodisperse spherical particles with a uniform size of 70 nm. Stringent control of synthesis time affords uniform and nanoscale particles and larger micron-sized particles can be obtained by elongating the reaction time to 24 h. The powder XRD (PXRD) patterns of the fluorescein-loaded ZIF-8 nanospheres are identical to the peaks assigned to a standard ZIF-8 crystal structure (Figure 1D). Fluorescein-loaded ZIF-8 spheres emit green fluorescence under irradiation and the peak emission wavelength is at 520 nm (Figure S2).

To identify the mode of fluorescein incorporation, different amounts of the fluorophore were introduced either during or after the formation of the ZIF-8 nanospheres. Increasing fluorescein applied during ZIF-8 formation (encapsulation) caused a red-shifting and increase in fluorescence intensity of the resulting nanospheres (Figure S2). In contrast, addition of fluorescein after the formation of the spheres (adsorption) resulted in a concomitant decrease in fluorescence with increased fluorophore concentration, and TEM images revealed particle aggregation (Figure 2A). This is likely a self-quenching effect due to surface clustering of the fluorophore, similar to that observed previously by Imhof *et al.*[46] We further verified the nature of incorporation by measuring the zeta-potentials of ZIF-8 micron-sized powder (BASF Basolite Z1200) and

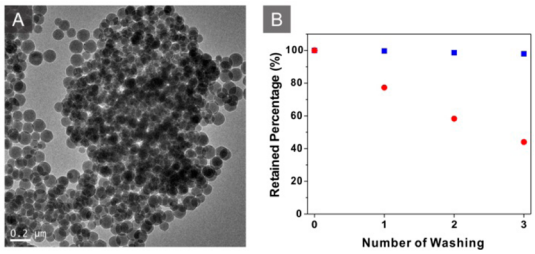

C

Sample name	Zeta- potential (mV)
Commercial ZIF-8 powder	32.6
Pure ZIF-8 nanospheres	31.4
Fluorescein-encapsulated ZIF-8 nanospheres	31.0
Fluorescein-adsorbed ZIF-8 nanospheres	22.9

Figure 2. (A) TEM image of aggregation of fluorescein-adsorbed ZIF-8 nanospheres; (B) PVP exchange results of encapsulated- (blue squares) and adsorbed- (red dots) ZIF-8 spheres; (C) zeta-potentials of ZIF-8 samples.

unmodified, fluorescein-encapsulated and fluorescein-adsorbed ZIF-8 nanospheres (Figure 2C). The micron-sized powder, the unmodified and the fluorescein-encapsulated ZIF-8 nanospheres had similar zeta-potentials of +32.6, +31.4, and +31.0 mV, respectively. In contrast, fluorescein-adsorbed nanospheres showed a decrease in the zeta-potential (+22.9 mV), confirming the surface adsorption of negatively charged fluorescein. Polyvinylpyrrolidone (PVP) surface adsorbant exchange was used to further confirm the encapsulation *versus* adsorption of the fluorophore. PVP has a high affinity to ZIF-8 and adsorption of PVP is restricted to the surface.[24,42] PVP treatment resulted in release of fluorescein into the solution for the fluorescein-adsorbed, but not the fluorescein-encapsulated nanospheres, thereby further confirming complete internalization of fluorescein in these spheres (Figure 2B).

Next, we explored the molecular mechanism of fluorescein encapsulation, which could be *in situ* trapped into the pores of the framework during crystal growth, or dynamically coordinated to the zinc centers *via* the deprotonated carboxylates of fluorescein. To evaluate this, we synthesized a fluorescein methyl ester,[47] lacking the carboxylate group (Figure 3A). UV−vis absorbance of the acid-disintegrated nanospheres were used to measure fluorescein incorporation and showed that the encapsulation efficiencies of fluorescein methyl ester and fluorescein were identical (Figure 3B). This observation confirms that the carboxylate group is not important for encapsulation, therefore supporting the *in situ* trapping mechanism. Furthermore, the amount of encapsulation varied linearly with the concentration of fluorescein in solution during synthesis, thereby providing uniform and tunable incorporation into the ZIF-8 framework (Scheme 2). The maximal loading amount is 1 wt %, with a 10% loading efficiency

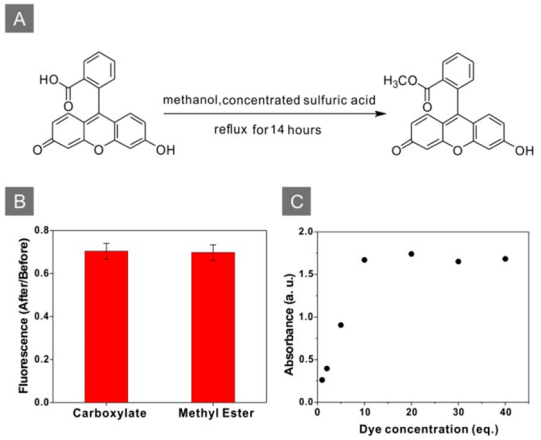

Figure 3. (A) Synthesis of fluorescein methyl ester; (B) comparison of dye encapsulation efficiencies of fluorescein carboxylate and fluorescein methyl ester *via* fluorimetry; (C) UV−vis absorbance of dissociated fluorescein-encapsulated ZIF-8, linear increase when dye concentration ≤10 equiv, and plateau when dye concentration >10 equiv; measured at peak wavelength (443 nm).

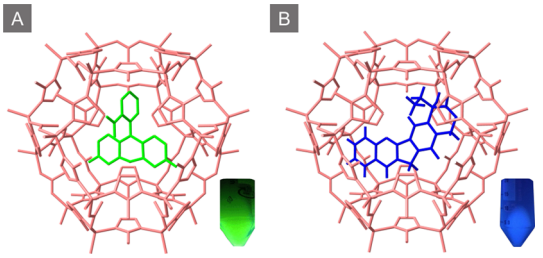

Scheme 2. Fluorescein (A) and Camptothecin (B) Encapsulated inside of ZIF-8 Frameworks.

(Figure 3C). The efficiency is comparable to those of existing MOF-based drug delivery systems.[16,28,33] We found that under the same synthetic condition, only negatively charged small molecules have a tendency to be encapsulated into the framework (*i.e.*, fluorescein, camptothecin), while neutral or positively charged molecules are poorly incorporated (*i.e.*, rhodamine 6G, bisphenol A). We demonstrate a unique approach to introduce diverse small molecules into nanomaterials through encapsulation of the small molecules into the ZIF-8 framework during synthesis. Unlike diffusion methods that have been used previously, this encapsulation method affords a more stable carrier with minimal premature release of the drug cargo.

To investigate the stability of ZIF-8 nanospheres under physiological and low pH conditions, the spheres were immersed in phosphate-buffered saline (PBS) solution (pH 7.4) and phosphate-buffered pH 6.0 solution. TEM analysis after one day revealed that the spheres in neutral PBS maintained their size and shape (Figures 4B and S3), whereas the particles in the pH 6.0 solution dissociated (Figure S4). Release of the fluorescein cargo from the ZIF-8 spheres was monitored by the fluorescence of the supernatants (Figure 4A). After one day, less than 10% of fluorescein release was detected

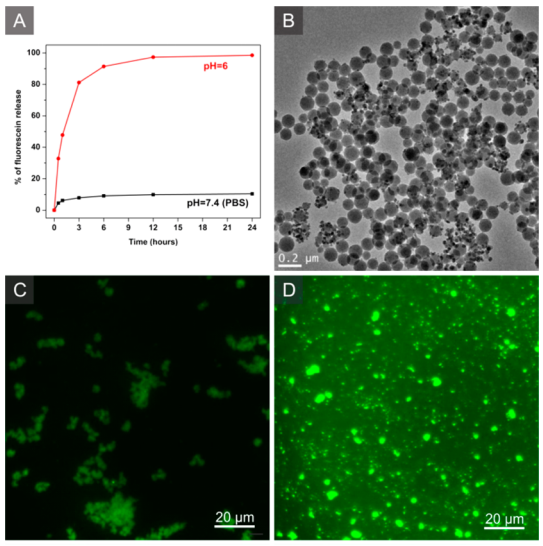

Figure 4. (A) Fluorescein release profile in PBS (black squares) and pH 6.0 buffer solution (red circles); (B) TEM image of fluorescein-encapsulated nanospheres dispersed in PBS for one day; (C) uncapped fluorescein-encapsulated ZIF-8 dispersed in cell medium; (D) CTAB-capped fluorescein-encapsulated ZIF-8 dispersed in cell medium.

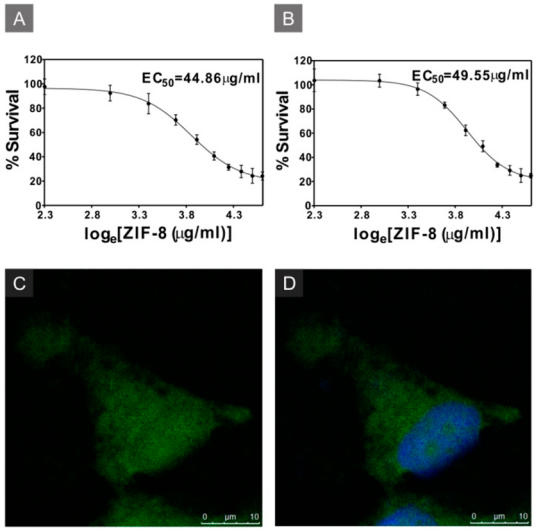

Figure 5. (A) Cell viability when incubated with CTAB-capped ZIF-8; (B) cell viability when incubated with uncapped ZIF-8; (C) FITC channel CLSM image on a single cell incubated with CTAB-capped fluorescein-encapsulated ZIF-8; (D) overlay image in FITC and DAPI channels on the same cell; cell nucleus stained by DAPI.

in PBS, whereas 50% of the encapsulated fluorescein was released within one hour of exposure to the acidic buffer. This pH-driven disintegration can be exploited for selective cargo release in acidic environments.

The cytotoxicity of the fluorescein-encapsulated ZIF-8 nanospheres was tested in MCF-7 breast cancer cells. To maintain the high dispersity of ZIF-8 spheres in the high ionic strength of the cell medium, we capped the spheres with cetyltrimethylammonium bromide (CTAB) and washed thoroughly to remove the unadsorbed CTAB. It has been reported that the hydro carbon tail of CTAB is adsorbed on the crystal surface *via* the hydrophobic effect.[48] Good dispersity of the spheres in cell medium was observed by fluorescent images and dynamic light scattering studies after the capping process (Figures 4C, D, and S5).

These capped nanospheres were incubated with MCF-7 breast cancer cells for 12 h at various concentrations and cell viability was measured using the MTT (3-(4,5-dimethylthiazol-2-yl)-2,5-diphenyltetrazolium bromide) reagent (Figure 5A). UV−vis absorbance spectra of pure ZIF-8, free fluorescein, and fluorescein-encapsulated ZIF-8 were obtained at various concentrations in PBS and showed no interference with MTT reading (Figure S6). The half maximal effective concentration (EC_{50}) of our ZIF-8 nanospheres was determined to be 45 μg/mL. This value is comparable to reported EC_{50} values for gold nanoparticles (varies from 5 to 1000 μg/mL), mesoporous silica nanomaterials (from 30 to 500 μg/mL), and the MILs (57 $\pm$ 11 μg/mL).[28,49,50] CTAB is a widely used cationic surfactant for nanoparticle synthesis;[51−54] however, it has been shown that CTAB could solubilize phospholipids and cause cell death.[55] We compared EC_{50} values for nanospheres with and without the CTAB capping process. There was no significant difference in EC_{50} values (Figure 5B), thereby confirming that most of the unbound CTAB was removed during the washing steps and the surface adsorbed CTAB did not increase the cytotoxicity of our spheres.[56]

The cellular uptake of fluorescein-loaded ZIF-8 spheres was evaluated by confocal laser scanning microscopy (CLSM). CLSM images confirmed successful uptake of the nanospheres into MCF-7 cells with uniformly dispersed fluorescence within the cell (Figure 5C, Figure S7). The particles appear to be uniformly dispersed throughout the cell, including the nucleus (Figure 5D). As negative controls, cells were incubated with pure ZIF-8 nanospheres without fluorescein encapsulation, micron-sized ZIF-8 particles encapsulating the same amount of fluorescein, as well as free fluorescein at the concentration found in the nanospheres. As expected, the cells incubated with pure ZIF-8 did not show any fluorescence, while the micron-sized ZIF-8-treated cells and the free fluorescein-treated cells showed faint fluorescence. Our data agrees with previous observations that micron-sized nanoparticles show poor cellular uptake.[57−59] These studies indicate that the uptake efficiencies are significantly higher when the fluorescein is incorporated into ZIF-8 nanospheres, as compared to larger particles or free fluorescein (Figure 6).

To further demonstrate the utility of these nanospheres for small molecule delivery into cells, we encapsulated camptothecin (CPT) into the ZIF-8 nanospheres. Camptothecin (CPT) is a quinolone alkaloid that induces apoptosis through inhibition of DNA topoisomerase I.[60] We demonstrate successful CPT encapsulation into the ZIF-8 nanospheres through blue fluorescence of the resulting

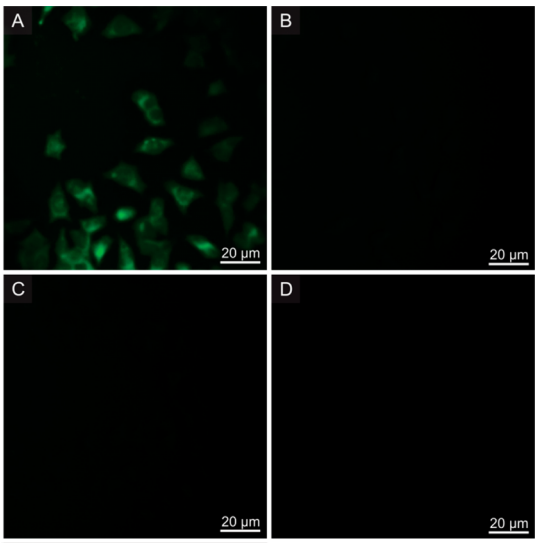

Figure 6. Fluorescence microscopy images of cells incubated with (A) 70 nm fluorescein-encapsulated ZIF-8; (B) micron-sized fluorescein-encapsulated ZIF-8; (C) free fluorescein; (D) pure ZIF-8.

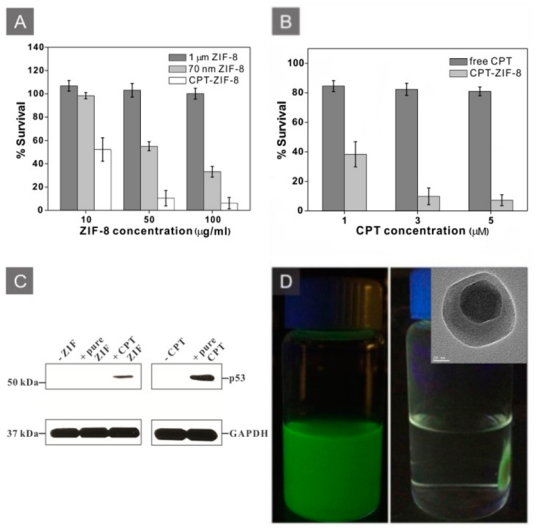

Figure 7. (A) Cell viability when incubated with micron-sized ZIF-8 (dark gray), 70 nm ZIF-8 (light gray), and CPT-encapsulated ZIF-8 (white); (B) cell viability when incubated with free CPT (dark gray), and CPT-encapsulated ZIF-8 (light gray) for 24 h; (C) Western blot on p53 level in MCF-7 cell lysates. p53 (53 kDa) levels were increased in CPT-encapsulated ZIF-8 and pure CPT treated cells. GAPDH levels (37 kDa) serve as a loading control; (D) Fe_3O_4@ZIF-8 nanospheres migrated to sides of a vial upon application of an external magnetic field; inset: TEM image of single Fe_3O_4@ZIF-8 nanosphere.

nanoparticles (Figure S8). The loading mechanism of CPT is also *in situ* encapsulation, whereby CPT is trapped inside the ZIF-8 framework (Scheme 2). The maximum loading amount is 2 wt %, while the loading efficiency is 30%. Pure ZIF-8 nanospheres, micron-sized CPT-encapsulated ZIF-8 particles, and CPT-encapsulated ZIF-8 nanospheres, were all evaluated for their effects on cell viability (Figure 7A). CPT-encapsulated ZIF-8 nanospheres showed a significant decrease in the EC_{50} value from fluorescein-ZIF-8 particles (from 45 to 22 μg/mL), suggesting successful delivery and release of cytotoxic CPT in cells. After 24 h of incubition, we compared cell survival upon exposure to free CPT and CPT-ZIF-8. The CPT-ZIF-8 treated cells showed increased cell death relative to free CPT treatment (Figure 7B). Effects of free CPT required 48 h to show an effect, thereby demonstrating that the ZIF-8 carrier accelerates the uptake of CPT into cells. To demonstrate successful release of CPT in cells, we monitored levels of p53 by Western blot analysis. CPT-induced cell death is known to be accompanied by increases in cellular p53 levels.[61] We show that treatment of MCF-7 cells with CPT-ZIF-8 and free CPT results in a concomitant increase in cellular p53 levels relative to untreated cells (Figure 7C).

To further demonstrate the versatility of our ZIF-8 scaffold, we introduced iron oxide nanoparticles during the synthesis.[62] The resulting ZIF-8 nanospheres have an iron oxide particle core and a fluorescein-encapsulated ZIF-8 shell. The crystallinity of ZIF-8 was preserved in Fe_3O_4@ZIF-8 nanospheres (Figure S9). Applying an external magnetic field causes directed migration of the fluorescent nanospheres (Figure 7D), suggesting that these particles can be selectively localized to specific tissues for targeted drug delivery.[63]

CONCLUSION

In summary, we have developed an ideal DDS based on ZIF-8 nanospheres, with 70 nm size that is optimal for cellular uptake. We demonstrate that the small molecules are encapsulated into the ZIF-8 frameworks, with high control of small-molecule loading. We conclude that this unique mechanism of incorporation is *in situ* trapping, and is thereby generalizable to small molecules of varying physicochemical properties. The cytotoxicity of the ZIF-8 sphere is moderate and comparable to other organic and inorganic drug carriers. We hypothesize that the particles are endocytosed by cells and the pH-triggered disintegration of the ZIF-8 framework in these acidic compartments results in drug release. We demonstrated the versatility of these ZIF-8 nanospheres by introducing the anticancer agent CPT and magnetic nanoparticles.

METHODS

Chemicals and Materials. Zinc nitrate hexahydrate ($Zn(NO_3)_2 \cdot 6H_2O$, ≥99%), 2-methylimidazole (99%), polyvinylpyrrolidone (PVP, M_w∼29 000) were purchased from Sigma-Aldrich and used without further purification. Fluorescein free acid (Reag. Ph. Eur.) was obtained from Fluka. Cetyltrimethylammonium bromide (CTAB, 98%) was obtained from Calbiochem. Camptothecin (CPT) was obtained from Alfa Aesar. Iron pentacarbonyl ($Fe(CO)_5$, 99.5%) was obtained from Acros. Methanol (HPLC grade) was obtained from Fisher Scientific. Trypsin-EDTA was purchased from Thermo Scientific. PBS buffer and serum-free phenol red RPMI 1640 cell medium were purchased from Corning

Cellgro. Serum-free RPMI 1640 clear cell medium was obtained from Invitrogen. P53 primary antibody and anti-rabbit IgG HRP-linked secondary antibody were purchased from Cell Signaling.

Characterization. Samples were prepared for TEM by diluting 50 μL sample solution to 500 μL and placing 2.0 μL droplets onto carbon-coated copper grids, then allowed to dry under a heat lamp. The instrument used for TEM was a JEOL JEM2010F operated at 200 kV. Samples were prepared for SEM by diluting 50 μL sample solution to 500 μL and placing a 1.0 μL droplet onto silicon wafer and drying under a heat lamp. The samples were then placed on silver glue atop double-sided copper tape on sample holder. SEM was performed using a JEOL JSM6340F. Samples for XRD were prepared by drying the sample solution in an oven and scraping the sample powder onto a sample holder. A Bruker D2 Phaser XRD instrument was used to obtain the powder XRD patterns. Samples for ICP-OES were prepared by dissolving oven dry sample powders in 5% nitric acid, and diluting to proper concentrations. ICP-OES was performed on a Perkin-Elmer optima 2100DV ICP-OEX spectrometer. Solution samples for zeta-potential were performed on a Malvern Zetasizer Nano ZS system. Normal fluorescence microscopy was performed on a Carl Zeiss Axio Observer A1 microscope. DLS was performed on a Wyatt DynaPro NanoStar system.

Synthesis of Fluorescein-Encapsulated ZIF-8. The synthesis of dye-loaded ZIF-8 is based on a previous procedure with some modifications.[64] For a typical synthesis, 150 mg of zinc nitrate hexahydrate and 330 mg of 2-methyl imidazole were weighed and transferred to a clean glass jar and scintillation vial, respectively. A volume of 7.15 mL of HPLC grade methanol was used to dissolve the solids in both containers. Subsequently, 0.15 mL (as 1 equivalent) 2 mg/mL fluorescein containing methanol solution was added into the zinc solution. The zinc solution showed a faint yellow color. The glass jar was equipped with a magnetic stir bar, and put onto stir plate. Next, as-prepared 2-methyl imidazole solution was poured into the jar and stirred for 5 min. The color of the solution immediately changed to a bright green color when 2-methyl imidazole was introduced, which indicated the deprotonation of fluorescein (Figure S1). Reaction solution became milky, implying the formation of ZIF-8 nanoparticles. Solution was centrifuged at 7000 rpm for 10 min to obtain the dye-loaded ZIF-8 after the reaction. As-synthesized nanoparticles were washed three more times with 10 mL of methanol to completely get rid of the unreacted reactants. Finally, yellow fluorescein-encapsulated ZIF-8 particles were suspended in 5 mL of methanol for storage and characterization. To acquire reaction yield of a typical synthesis, as-synthesized ZIF-8 nanoparticles were completely decomposed by 5% nitric acid solution, and zinc metal concentration was monitored by ICP-OES. It shows that 15 mg of ZIF-8 can be obtained for a single synthesis.

Synthesis of Camptothecin-Encapsulated ZIF-8. The synthesis was conducted similar to the synthesis of fluorescein-loaded ZIF-8 described above. The only change was to introduce 1 mg of camptothecin (CPT) into the zinc solution instead of fluorescein at the beginning.

Synthesis of Fe_3O_4@Fluorescein-Encapsulated ZIF-8. The synthesis of PVP-coated iron oxide was based on a published procedure without any changes.[62] A total of 400 μL of iron pentacarbonyl was injected into a 160 °C DMF solution which contained 4 g of PVP. The reaction was kept for 3 h, and then as-synthesized iron oxide particles were washed by methanol and dispersed in 10 mL of methanol. The synthesis of ZIF-8 shell was similar to the synthesis of fluorescein-loaded ZIF-8 described above. The only change was to introduce 50 μL of iron oxide solution to the zinc solution at the beginning of the synthesis.

Synthesis of Fluorescein Methyl Ester. The synthesis was based on a previous report.[47] Briefly, 4 mL of concentrated sulfuric acid was added to a suspension of 5 g of fluorescein in 15 mL of methanol. The solution was refluxed for 14 h with an addition funnel packed with 3 Å molecular sieves. The resulting red mixture was cooled by 5 g of ice, and neutralized by 5 g of sodium bicarbonate. The suspension was filtered and washed with water, 100 mL of 2% aqueous sodium bicarbonate, 100 mL of 1% HOAc, and finally washed with water. The fluorescein methyl ester was obtained as a red solid after drying the sample in an oven. The product was determined to be fluorescein methyl ester using mass spectrometry and NMR.

Visible Light Absorption Spectroscopy. As-synthesized dye-encapsulated ZIF-8 was spun down, and the supernatant was removed. Then 5 mL of pH 2 hydrochloride solution was added into the centrifuge tube to fully disintegrate the ZIF-8 particles. The resulting clear yellow dye solution was transferred to a 1 cm glass cuvette to measure the visible light absorption spectrum on a Thermo Scientific NanoDrop 2000c.

Fluorimetry. Three milliliters of particle solution was transferred to a 1 cm glass cuvette. The excitation wavelength was set at 495 nm. The emission light spectrum was detected on a Horiba Jobin Yvon FL3-22 Fluorolog spectrometer.

PVP Exchange. As-synthesized ZIF-8 was dispersed in 10 mL of 5% PVP methanol solution, left for 10 min, then centrifuged down to obtain the supernatant. The fluorimetry measurement was taken on the supernatant. This PVP exchange was repeated 2 more times.

ZIF-8 Decomposition. Two as-synthesized dye-encapsulated ZIF-8 samples from the same batch were suspended in PBS and phosphate buffered pH 6.0 solution, respectively. At specific time points, the samples were spun down and the fluorescence of the supernatant was measured. ZIF-8 samples were resuspended in fresh methanol with the same solution volume.

CTAB Capping on ZIF-8. As-synthesized ZIF-8 was dispersed in 10 mL of methanol which contained 100 mg of CTAB, then centrifuged at 7000 rpm for 10 min to obtain CTAB-capped ZIF-8. The particles were washed 3 more times with 10 mL of methanol to fully wash off unadsorbed CTAB.

MTT Assay. A total of 100 μL of MCF-7 cell solution was pipetted into the wells of a 96-well plate to provide a cell density of 30 000 cells per well. The plate was then incubated for 36 h at 37 °C in 5% CO_2 atmosphere. After removal of the cell medium, as-synthesized particles or free CPT in DMSO were mixed with 100 μL of RPMI 1640 cell medium and pipetted into each well. The whole plate was incubated for another 24 h, after which the cell medium was removed. Ten microliters of 0.5% MTT reagent ((3-(4,5)-dimethylthiazol-2-yl)-2,5-diphenyl tetrazolium bromide) in PBS buffer mixed with 100 μL of clear cell medium was transferred to each well. The reagent was quenched by 100 μL of 10% SDS in 0.1% autoclaved hydrochloride solution after 4 h incubation. The plate was incubated for another 6 h and the absorbance was read at 570 nm using a Molecular Devices Spectramax M5 plate reader.

Confocal Laser Scanning Microscopy. A total of 500 μL of MCF-7 cell suspension was transferred to wells on a microscope slide. After incubating the slide for 24 h, the medium in each well was removed. As-synthesized dye-encapsulated particles dispersed in 500 μL of RPMI 1640 clear medium were introduced to each well to make final particle concentration of 50 μg/mL and incubated for 4 h. The medium was removed, and cells were washed 3 times with PBS and 3 times with cold methanol, and finally fixed with cold methanol. Then 250 μL of 300 nM DAPI in PBS was added to each well, and incubated for 5 min. Afterward, each well was washed 5 times with PBS. The whole slide was covered by a glass coverslip and imaged using a Leica SP5 microscope.

Western Blot Analysis. Near fully confluent MCF-7 cells were treated with 100 μg/mL particles or 10 μM free CPT overnight before they were scraped, washed and pelleted, and lysed by sonication in PBS. Soluble lysates were obtained by ultracentrifugation and protein concentrations were normalized to 1.5 mg/mL. These lysates were separated by SDS-PAGE (130 mV, 80 min), and transferred to nitrocellulose membranes (80 mV, 120 min). The membrane was washed with TBST, blocked with milk and exposed to p53 primary antibody (1:1000) in TBST overnight at 4 °C. After a washing step with TBST, the membrane was exposed to anti-rabbit–HRP conjugated secondary antibody (1:3000) in TBST for 2 h at room temperature. The membrane was washed with TBST before being treated with HRP super signal chemiluminescence reagents and exposed to film for 5 min before development, using a Kodak X-OMAT 2000A processor.

Conflict of Interest: The authors declare no competing financial interest.

Acknowledgment. This work is supported by the Damon Runyon Cancer Research Foundation (DRR-18-12) (E. Weerapana), the Smith Family Foundation (E. Weerapana) and Boston College. Thanks to A. Platt for supplying materials. Special thanks to C. Dhital, B. Judson and Gao Lab in Boston College, Prof. D. Qu and Dr. D. Zheng from UMass-Boston for help with instrumentation.

Supporting Information Available: Figures including reaction solution color change, CPT-ZIF-8 under UV lamp, fluorimetry spectra of fluorescein-ZIF-8, TEM images of ZIF-8 in physiological fluids and dissociated ZIF-8 in acidic buffer, DLS of ZIF-8 in methanol, UV–vis spectra of MTT, CLSM images of nontreated or treated cells, and XRD patterns of Fe_3O_4@ZIF-8. This material is available free of charge *via* the Internet at http://pubs.acs.org.

REFERENCES AND NOTES

1. Cho, K.; Wang, X.; Nie, S.; Chen, Z. G.; Shin, D. M. Therapeutic Nanoparticles for Drug Delivery in Cancer. *Clin. Cancer Res.* **2008**, *14*, 1310–1316.
2. Faraji, A. H.; Wipf, P. Nanoparticles in Cellular Drug Delivery. *Biorg. Med. Chem.* **2009**, *17*, 2950–2962.
3. Kong, G.; Braun, R. D.; Dewhirst, M. W. Hyperthermia Enables Tumor-Specific Nanoparticle Delivery: Effect of Particle Size. *Cancer Res.* **2000**, *60*, 4440–4445.
4. Trewyn, B. G.; Slowing, I. I.; Giri, S.; Chen, H.-T.; Lin, V. S. Y. Synthesis and Functionalization of a Mesoporous Silica Nanoparticle Based on the Sol–Gel Process and Applications in Controlled Release. *Acc. Chem. Res.* **2007**, *40*, 846–853.
5. Petros, R. A.; DeSimone, J. M. Strategies in the Design of Nanoparticles for Therapeutic Applications. *Nat. Rev. Drug Discovery* **2010**, *9*, 615–627.
6. Mallouk, T. E.; Yang, P. D. Chemistry at the Nano-Bio Interface. *J. Am. Chem. Soc.* **2009**, *131*, 7937–7939.
7. Xu, Z. P.; Zeng, Q. H.; Lu, G. Q.; Yu, A. B. Inorganic Nanoparticles as Carriers for Efficient Cellular Delivery. *Chem. Eng. Sci.* **2006**, *61*, 1027–1040.
8. Murphy, C. J.; Gole, A. M.; Stone, J. W.; Sisco, P. N.; Alkilany, A. M.; Goldsmith, E. C.; Baxter, S. C. Gold Nanoparticles in Biology: Beyond Toxicity to Cellular Imaging. *Acc. Chem. Res.* **2008**, *41*, 1721–1730.
9. Di Pasqua, A. J.; Sharma, K. K.; Shi, Y. L.; Toms, B. B.; Ouellette, W.; Dabrowiak, J. C.; Asefa, T. Cytotoxicity of Mesoporous silica Nanomaterials. *J. Inorg. Biochem.* **2008**, *102*, 1416–1423.
10. Cobley, C. M.; Chen, J. Y.; Cho, E. C.; Wang, L. V.; Xia, Y. N. Gold Nanostructures: A Class of Multifunctional Materials for Biomedical Applications. *Chem. Soc. Rev.* **2011**, *40*, 44–56.
11. Paxton, W. F.; Sen, A.; Mallouk, T. E. Motility of Catalytic Nanoparticles through Self-generated Forces. *Chem.—Eur. J.* **2005**, *11*, 6462–6470.
12. Tang, F.; Li, L.; Chen, D. Mesoporous Silica Nanoparticles: Synthesis, Biocompatibility and Drug Delivery. *Adv. Mater.* **2012**, *24*, 1504–1534.
13. Boisselier, E.; Astruc, D. Gold Nanoparticles in Nanomedicine: Preparations, Imaging, Diagnostics, Therapies and Toxicity. *Chem. Soc. Rev.* **2009**, *38*, 1759–1782.
14. Xie, J.; Lee, S.; Chen, X. Nanoparticle-Based Theranostic Agents. *Adv. Drug Delivery Rev.* **2010**, *62*, 1064–1079.
15. Vallet-Regí, M.; Balas, F.; Arcos, D. Mesoporous Materials for Drug Delivery. *Angew. Chem., Int. Ed.* **2007**, *46*, 7548–7558.
16. Della Rocca, J.; Liu, D.; Lin, W. Nanoscale Metal–Organic Frameworks for Biomedical Imaging and Drug Delivery. *Acc. Chem. Res.* **2011**, *44*, 957–968.
17. Rowsell, J. L.; Yaghi, O. M. Strategies for Hydrogen Storage in Metal-Organic Frameworks. *Angew. Chem., Int. Ed.* **2005**, *44*, 4670–4679.
18. Dincă, M.; Long, J. R. Hydrogen Storage in Microporous Metal-Organic Frameworks with Exposed Metal Sites. *Angew. Chem., Int. Ed.* **2008**, *47*, 6766–6779.
19. Chen, B.; Ma, S.; Hurtado, E. J.; Lobkovsky, E. B.; Liang, C.; Zhu, H.; Dai, S. Selective Gas Sorption within a Dynamic Metal-Organic Framework. *Inorg. Chem.* **2007**, *46*, 8705–8709.
20. Chen, B.; Xiang, S.; Qian, G. Metal–Organic Frameworks with Functional Pores for Recognition of Small Molecules. *Acc. Chem. Res.* **2010**, *43*, 1115–1124.
21. Jiang, H.-L.; Tatsu, Y.; Lu, Z.-H.; Xu, Q. Non-, Micro-, and Mesoporous Metal–Organic Framework Isomers: Reversible Transformation, Fluorescence Sensing, and Large Molecule Separation. *J. Am. Chem. Soc.* **2010**, *132*, 5586–5587.
22. Jiang, H.-L.; Xu, Q. Porous Metal-Organic Frameworks as Platforms for Functional Applications. *Chem. Commun.* **2011**, *47*, 3351–3370.
23. Lee, J.; Farha, O. K.; Roberts, J.; Scheidt, K. A.; Nguyen, S. T.; Hupp, J. T. Metal-Organic Framework Materials as Catalysts. *Chem. Soc. Rev.* **2009**, *38*, 1450–1459.
24. Kuo, C.-H.; Tang, Y.; Chou, L.-Y.; Sneed, B. T.; Brodsky, C. N.; Zhao, Z.; Tsung, C.-K. Yolk-Shell Nanocrystal@ZIF-8 Nanostructures for Gas-Phase Heterogeneous Catalysis with Selectivity Control. *J. Am. Chem. Soc.* **2012**, *134*, 14345–14348.
25. Rieter, W. J.; Taylor, K. M. L.; An, H.; Lin, W.; Lin, W. Nanoscale Metal–Organic Frameworks as Potential Multimodal Contrast Enhancing Agents. *J. Am. Chem. Soc.* **2006**, *128*, 9024–9025.
26. Taylor, K. M. L.; Rieter, W. J.; Lin, W. Manganese-Based Nanoscale Metal–Organic Frameworks for Magnetic Resonance Imaging. *J. Am. Chem. Soc.* **2008**, *130*, 14358–14359.
27. Rieter, W. J.; Pott, K. M.; Taylor, K. M. L.; Lin, W. Nanoscale Coordination Polymers for Platinum-Based Anticancer Drug Delivery. *J. Am. Chem. Soc.* **2008**, *130*, 11584–11585.
28. Horcajada, P.; Chalati, T.; Serre, C.; Gillet, B.; Sebrie, C.; Baati, T.; Eubank, J. F.; Heurtaux, D.; Clayette, P.; Kreuz, C.; *et al.* Porous Metal-Organic-Framework Nanoscale Carriers as a Potential Platform for Drug Delivery and Imaging. *Nat. Mater.* **2010**, *9*, 172–178.
29. Horcajada, P.; Serre, C.; Vallet-Regí, M.; Sebban, M.; Taulelle, F.; Férey, G. Metal-Organic Frameworks as Efficient Materials for Drug Delivery. *Angew. Chem., Int. Ed.* **2006**, *45*, 5974–5978.
30. An, J.; Geib, S. J.; Rosi, N. L. Cation-Triggered Drug Release from a Porous Zinc–Adeninate Metal–Organic Framework. *J. Am. Chem. Soc.* **2009**, *131*, 8376–8377.
31. Liédana, N.; Galve, A.; Rubio, C.; Téllez, C.; Coronas, J. CAF@ZIF-8: One-Step Encapsulation of Caffeine in MOF. *ACS Appl. Mater. Interfaces* **2012**, *4*, 5016–5021.
32. Imaz, I.; Hernando, J.; Ruiz-Molina, D.; Maspoch, D. Metal-Organic Spheres as Functional Systems for Guest Encapsulation. *Angew. Chem., Int. Ed.* **2009**, *48*, 2325–2329.
33. Imaz, I.; Rubio-Martínez, M.; García-Fernández, L.; García, F.; Ruiz-Molina, D.; Hernando, J.; Puntes, V.; Maspoch, D. Coordination Polymer Particles as Potential Drug Delivery Systems. *Chem. Commun.* **2010**, *46*, 4737–4739.
34. Yanai, N.; Granick, S. Directional Self-assembly of a Colloidal Metal-Organic Framework. *Angew. Chem., Int. Ed.* **2012**, *51*, 5638–5641.
35. Yanai, N.; Sindoro, M.; Yan, J.; Granick, S. Electric Field-Induced Assembly of Monodisperse Polyhedral Metal–Organic Framework Crystals. *J. Am. Chem. Soc.* **2012**, *135*, 34–37.
36. Chithrani, B. D.; Ghazani, A. A.; Chan, W. C. W. Determining the Size and Shape Dependence of Gold Nanoparticle Uptake into Mammalian Cells. *Nano Lett.* **2006**, *6*, 662–668.
37. Sun, C.-Y.; Qin, C.; Wang, X.-L.; Yang, G.-S.; Shao, K.-Z.; Lan, Y.-Q.; Su, Z.-M.; Huang, P.; Wang, C.-G.; Wang, E.-B. Zeolitic Imidazolate Framework-8 as Efficient pH-sensitive Drug Delivery Vehicle. *Dalton Trans.* **2012**, *41*, 6906–6909.
38. Taylor-Pashow, K. M. L.; Della Rocca, J.; Xie, Z.; Tran, S.; Lin, W. Postsynthetic Modifications of Iron-Carboxylate Nanoscale Metal–Organic Frameworks for Imaging and Drug Delivery. *J. Am. Chem. Soc.* **2009**, *131*, 14261–14263.
39. Keskin, S.; Kzlel, S. Biomedical Applications of Metal Organic Frameworks. *Ind. Eng. Chem. Res.* **2011**, *50*, 1799–1812.
40. Park, K. S.; Ni, Z.; Côté, A. P.; Choi, J. Y.; Huang, R.; Uribe-Romo, F. J.; Chae, H. K.; O'Keeffe, M.; Yaghi, O. M.

Exceptional Chemical and Thermal Stability of Zeolitic Imidazolate Frameworks. *Proc. Natl. Acad. Sci. U. S. A.* **2006**, *103*, 10186–10191.
41. Broadley, M. R.; White, P. J.; Hammond, J. P.; Zelko, I.; Lux, A. Zinc in Plants. *New Phytol.* **2007**, *173*, 677–702.
42. Lu, G.; Li, S.; Guo, Z.; Farha, O. K.; Hauser, B. G.; Qi, X.; Wang, Y.; Wang, X.; Han, S.; Liu, X.; *et al.* Imparting Functionality to a Metal–Organic Framework Material by Controlled Nanoparticle Encapsulation. *Nat. Chem.* **2012**, *4*, 310–316.
43. Ke, F.; Yuan, Y.-P.; Qiu, L.-G.; Shen, Y.-H.; Xie, A.-J.; Zhu, J.-F.; Tian, X.-Y.; Zhang, L.-D. Facile Fabrication of Magnetic Metal-Organic Framework Nanocomposites for Potential Targeted Drug Delivery. *J. Mater. Chem.* **2011**, *21*, 3843–3848.
44. Morris, W.; Doonan, C. J.; Furukawa, H.; Banerjee, R.; Yaghi, O. M. Crystals as Molecules: Postsynthesis Covalent Functionalization of Zeolitic Imidazolate Frameworks. *J. Am. Chem. Soc.* **2008**, *130*, 12626–12627.
45. Karagiaridi, O.; Lalonde, M. B.; Bury, W.; Sarjeant, A. A.; Farha, O. K.; Hupp, J. T. Opening ZIF-8: A Catalytically Active Zeolitic Imidazolate Framework of Sodalite Topology with Unsubstituted Linkers. *J. Am. Chem. Soc.* **2012**, *134*, 18790–18796.
46. Imhof, A.; Megens, M.; Engelberts, J. J.; de Lang, D. T. N.; Sprik, R.; Vos, W. L. Spectroscopy of Fluorescein (FITC) Dyed Colloidal Silica Spheres. *J. Phys. Chem. B* **1999**, *103*, 1408–1415.
47. Adamczyk, M.; Grote, J.; Moore, J. A. Chemoenzymatic Synthesis of 3′-O-(Carboxyalkyl)fluorescein Labels. *Bioconjugate Chem.* **1999**, *10*, 544–547.
48. Pan, Y.; Heryadi, D.; Zhou, F.; Zhao, L.; Lestari, G.; Su, H.; Lai, Z. Tuning the Crystal Morphology and Size of Zeolitic Imidazolate Framework-8 in Aqueous Solution by Surfactants. *CrystEngComm* **2011**, *13*, 6937–6940.
49. Pan, Y.; Neuss, S.; Leifert, A.; Fischler, M.; Wen, F.; Simon, U.; Schmid, G.; Brandau, W.; Jahnen-Dechent, W. Size-Dependent Cytotoxicity of Gold Nanoparticles. *Small* **2007**, *3*, 1941–1949.
50. He, Q.; Zhang, Z.; Gao, Y.; Shi, J.; Li, Y. Intracellular Localization and Cytotoxicity of Spherical Mesoporous Silica Nano- and Microparticles. *Small* **2009**, *5*, 2722–2729.
51. Johnson, C. J.; Dujardin, E.; Davis, S. A.; Murphy, C. J.; Mann, S. Growth and Form of Gold Nanorods Prepared by Seed-Mediated, Surfactant-directed Synthesis. *J. Mater. Chem.* **2002**, *12*, 1765–1770.
52. Huo, Q.; Margolese, D. I.; Stucky, G. D. Surfactant Control of Phases in the Synthesis of Mesoporous Silica-Based Materials. *Chem. Mater.* **1996**, *8*, 1147–1160.
53. Chen, D.-H.; Wu, S.-H. Synthesis of Nickel Nanoparticles in Water-in-Oil Microemulsions. *Chem. Mater.* **2000**, *12*, 1354–1360.
54. Lee, K. T.; Jung, Y. S.; Oh, S. M. Synthesis of Tin-Encapsulated Spherical Hollow Carbon for Anode Material in Lithium Secondary Batteries. *J. Am. Chem. Soc.* **2003**, *125*, 5652–5653.
55. Gérardin, C.; Reboul, J.; Bonne, M.; Lebeau, B. Ecodesign of Ordered Mesoporous Silica Materials. *Chem. Soc. Rev.* **2013**, *42*, 4217–4255.
56. Alkilany, A. M.; Nagaria, P. K.; Hexel, C. R.; Shaw, T. J.; Murphy, C. J.; Wyatt, M. D. Cellular Uptake and Cytotoxicity of Gold Nanorods: Molecular Origin of Cytotoxicity and Surface Effects. *Small* **2009**, *5*, 701–708.
57. Rejman, J.; Oberle, V.; Zuhorn, I. S.; Hoekstra, D. Size-dependent Internalization of Particles *via* the Pathways of Clathrin- and Caveolae-Mediated Endocytosis. *Biochem. J.* **2004**, *377*, 159–169.
58. Zhang, S.; Li, J.; Lykotrafitis, G.; Bao, G.; Suresh, S. Size-Dependent Endocytosis of Nanoparticles. *Adv. Mater.* **2009**, *21*, 419–424.
59. Osaki, F.; Kanamori, T.; Sando, S.; Sera, T.; Aoyama, Y. A Quantum Dot Conjugated Sugar Ball and Its Cellular Uptake. On the Size Effects of Endocytosis in the Subviral Region. *J. Am. Chem. Soc.* **2004**, *126*, 6520–6521.
60. Hsiang, Y. H.; Hertzberg, R.; Hecht, S.; Liu, L. F. Camptothecin Induces Protein-Linked DNA Breaks *via* Mammalian DNA Topoisomerase I. *J. Biol. Chem.* **1985**, *260*, 14873–14878.
61. Liu, W.; Zhang, R. Upregulation of p21WAF1/CIP1 in Human Breast Cancer Cell Lines MCF-7 and MDA-MB-468 Undergoing Apoptosis Induced by Natural Product Anticancer Drugs 10-Hydroxycamptothecin and Camptothecin through p53-dependent and Independent Pathways. *Int. J. Oncol.* **1998**, *12*, 793–804.
62. Huang, J.; Bu, L.; Xie, J.; Chen, K.; Cheng, Z.; Li, X.; Chen, X. Effects of Nanoparticle Size on Cellular Uptake and Liver MRI with Polyvinylpyrrolidone-Coated Iron Oxide Nanoparticles. *ACS Nano* **2010**, *4*, 7151–7160.
63. Gao, J.; Gu, H.; Xu, B. Multifunctional Magnetic Nanoparticles: Design, Synthesis, and Biomedical Applications. *Acc. Chem. Res.* **2009**, *42*, 1097–1107.
64. Venna, S. R.; Jasinski, J. B.; Carreon, M. A. Structural Evolution of Zeolitic Imidazolate Framework-8. *J. Am. Chem. Soc.* **2010**, *132*, 18030–18033.